IEEE Access
Multidisciplinary | Rapid Review | Open Access Journal

Received May 12, 2021, accepted May 24, 2021, date of publication June 8, 2021, date of current version June 28, 2021.

Digital Object Identifier 10.1109/ACCESS.2021.3087505

A Robust Observer for Sensor Faults Estimation on n-DOF Manipulator in Constrained Framework Environment

HOAI VU ANH TRUONG[1], HOAI AN TRINH[1], DUC THIEN TRAN[2], (Member, IEEE), AND KYOUNG KWAN AHN[1], (Senior Member, IEEE)

[1]School of Mechanical Engineering, University of Ulsan, Ulsan 44610, South Korea
[2]Automatic Control Department, Ho Chi Minh City University of Technology and Education, Ho Chi Minh City 700000, Vietnam

Corresponding author: Kyoung Kwan Ahn (kkahn@ulsan.ac.kr)

This work was supported by the Basic Science Program through the National Research Foundation of Korea (NRF) by the Ministry of Science and ICT, South Korea, under Grant NRF 2020R1A2B5B03001480.

ABSTRACT This paper presents a fault-tolerant control (FTC) based on impedance control and full state feedback backstepping sliding mode control (FBSMC) algorithm for an n degree of freedoms (n-DOF) serial hydraulic manipulator under the presence of matched and mismatched uncertainties and sensor faults in the constrained framework. These faulty signals, generated from unknown constant or time-variant offset values, happen on both manipulator joint angles and force sensors; thereby degrading the system performance. Therefore, to address both matched and mismatched uncertainties and signal faults, the system dynamics subjects to the sensor faults is mathematically modeled. Then, the robust fault estimation algorithm based on extended state observer (ESO) is proposed to estimate the system state and faulty signals for the FTC design to achieve the force and position tracking performance. System stability of the proposed control scheme is theoretically proven by performing Lyapunov theorems. Finally, comparative simulation results are given on a 3-DOF serial hydraulic manipulator to evaluate the effectiveness of the proposed fault estimation and FTC methodology.

INDEX TERMS Sensor fault estimation, extended state observer (ESO), fault-tolerant control (FTC), force control, impedance control.

I. INTRODUCTION

As the rapid development in the field of automation, system analysis and control strategy design have become topics of interest in control research area in recent years. Several methodologies were proposed to exhibit the tracking performance for multi-input-multi-output nonlinear systems [1]–[4] such as advanced control algorithms [5]–[7], fractional-order control [8]–[10], intelligent techniques [11]–[15], or even optimization [16], [17] for robotic manipulators.

Although the tracking performance could be achieved, all automatically controlled systems may be inevitably subjected to faults caused by system elements, actuator, or sensor in practice. The actuator and sensor faults are more popular due to the coupled association with the design of control algorithms. As the highly coupled nonlinear characteristics, the actuator fault causes obvious effects on the system dynamics; therefore, they can be easily detected through monitoring abnormal system performances. Following the literature of actuator fault detection and isolation, and estimation, such fault can be considered as matched or mismatched disturbances and observed by using observers such as extended state observers (ESO) [15], [18], [19], disturbance observers (DO) [12], [20]–[22], uncertainty and disturbance estimator (UDE) [23], [24], time-delayed estimation (TDE) [25]–[27], super-twisting algorithm [28], Kalman estimators [29], unknown input observer [30], [31], etc. Then, Fault-tolerant control (FTC) that combines these observers compensation with advanced control algorithms such as active disturbance rejection control (ADRC) [32], [33], adaptive algorithms [34]–[36], or high robust gains can be employed to address the influence of the actuator fault.

Meanwhile, the sensor fault is generated from unknown constant or time-variant offset added to the measured signal and does not cause obvious influences. Due to the

The associate editor coordinating the review of this manuscript and approving it for publication was Moussa Boukhnifer.

additive measurements, the system behavior is the same as the fault-free condition, but the measured feedback signal cannot present the true value of the system states. However, wrong feedback signal results in an unsuitable execution in terms of physical interactions; thus, being able to cause severe problems such as system performance deterioration and instability, loss of information fidelity unless promptly addressing [37]. Therefore, the main objective is to critically achieve a fast and reliable sensor fault detection and estimation. Various methodologies for this topic were proposed. Nguyen *et al.* [38], [39] employed a nonlinear UIO to detect the sensor fault on the mini motion package EHS. Nahian *et al.* [40] used an extended Kalman-Bucy unknown input observer to detect the sensor fault and estimate the system state and developed an FTC for the EHS. Brambilla *et al.* [41] and Capisani *et al.* [42] conducted a bank of observers based on the SMO for sensor fault detection and isolation on serial manipulators. Pang *et al.* constructed an active FTC with the SMO to address the influence of sensor fault on automobile active suspension systems. Paviglianiti *et al.* [43] proposed a robust fault detection based on traditional Luenberger observer to detect and isolate the sensor faults on the multi-output system. Various approaches can be referred from [44]–[46]. The UIO and SMO are usually employed for fault detection and isolation; however, the complicated calculation using LMI and requirement of coordinate transformation increase the difficulty for high-order nonlinear systems. The sensor faults, in another aspect, can be considered as extended states of the controlled system. Therefore, other methods, such as using observers or adaptive laws, can be constructed to effectively estimate the magnitude of the faulty signals. The DO and UDE, or TDE have shown their effectiveness in disturbance estimation and rejection; however, the involvement of nominal system dynamics in constructing the adaptive laws complicates the estimation design and results in more computation. Conversely, the ESO only considers the system state and estimated state for adaptive laws construction. This method is easier to implement rather than the other one but shows its effectiveness in estimating unmeasurable variables. Sun *et al.* [47] proposed an adaptive observer to estimate the sensor fault for the active FTC design of linear multi-agent systems. By transferring to another form [48], the sensor fault was rearranged with the same channel as the actuator fault. Khebbache *et al.* [49] derived an FTC-based backstepping technique for a class of multi-input-multi-output nonlinear systems, in which adaptive laws for fault estimation were involved in each step of the recursive design. However, the approach supposed that all first measured outputs were fault-free. Moreover, by following the previous literature, most approaches just concerned the system sensor faults subjected to free motion. In other words, there is no achievement of sensor fault estimation algorithm in terms of constrained motion, in which force sensor used for interaction monitoring may be faulty when the manipulator is in contact with the environment such as polishing, welding, cutting, or so on.

Motivated from the above analyses of the favorable control methods, this paper proposes an FTC for an n-degree-of-freedom (n-DOF) serial hydraulic manipulator under the presence of sensor faults in the constrained framework for the first time. To address the sensor faults effect, and furthermore for matched uncertainty, a robust fault estimation based on ESO is proposed to estimate the system state and faulty signal residual. Based on the estimated parameters, the FTC is constructed so as to achieve the system output performance. The main contributions of this current work can be listed as

1) To the best of our knowledge, this is the first time the proposed FTC is examined on the hydraulic robotic manipulator subject to constrained framework motion in which both joint angle sensors fault, and force sensor fault are considered.
2) The robust sensor faults estimation based on ESO is constructed, which concerns the residual signal faults as extended state variables to be estimated. Based on the estimated residuals, the actual system state can be obtained for the FTC design. Besides, the matched uncertainty is also involved in the fault estimation design process.
3) The stability of the robust fault estimation and the closed-loop system are theoretically proven by performing Lyapunov theorems. Additionally, numerical simulations are provided to evidently demonstrate the effectiveness of the proposed FTC scheme.

The rest of the paper is organized as the following: Section II describes the impedance dynamics and whole system behavior of the n-DOF serial hydraulic manipulator with the presence of sensor faults through a mathematical model. Based on the system modeling, the robust fault estimation and FTC are derived in Section III. The stability proof of the closed-loop system is discussed in Section IV. Numerical simulations and discussions are explained in Section V. Finally, Section VI gives some conclusions and future works.

II. PROBLEM FORMULATION

A. IMPEDANCE CONTROL

During the interaction, the environment sets constraints on the geometric paths that can be followed by the end effector. This situation is generally referred to as constrained motion [50]. There are two paradigms named direct force control and indirect force control. The direct force control mainly refers to hybrid position/force. This technique is employed in the point of industrial applications in which a task space is partitioned into force sub-space and position sub-space determined by a switch matrix. However, low robustness and instability when operating in changeable or wavy surfaces are drawbacks of this strategy. Besides, information of constraint that is not always available is required to achieve good accuracy. In this sense, the indirect force control, normally known as impedance control, is more preferable to construct the outer/inner force/position-based cascade control. The detail

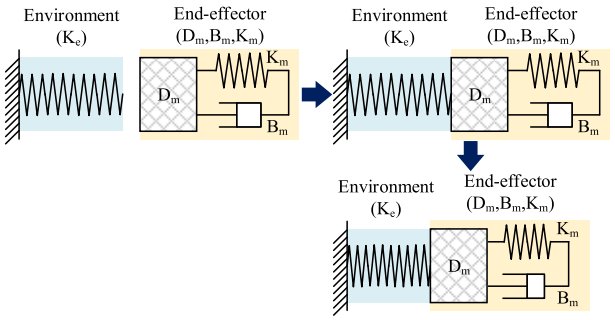

FIGURE 1. Illustration of physical interaction between the end-effector with the environment.

of constraint is not necessary since the methodology does not require the switch matrix to partition workspace like the direct force method. Therefore, in this study, position-based impedance control (PB-IC) is preferred to deal with a tradeoff between force tracking and position tracking in a constrained framework. The physical interaction between the manipulator end-effector and environment based on the PB-IC is illustrated in FIGURE 1.

Assumption 1: The environment is assumed to be rigid, with no damping during the interaction, and is presented by a stiff spring.

From the deformation of the environment spring, the interactive force between the end-effector and environment is expressed by:

$$\mathbf{F}_{ext} = -K_e \left(\mathbf{X}_a - \mathbf{X}_e\right) \tag{1}$$

where $\mathbf{X}_a \in R^3$ and $\mathbf{X}_e \in R^3$ denote the end-effector position and environment location, respectively; K_e is the environment stiffness.

The conventional PB-IC, presenting the coupled interaction of the robot manipulator with the environment, is redesigned from [51] by the second-order mass-spring-damper mechanisms as

$$\mathbf{D}_m \Delta\ddot{\mathbf{X}} + \mathbf{B}_m \Delta\dot{\mathbf{X}} + \mathbf{K}_m \Delta\mathbf{X} = \mathbf{u}_{imp} \tag{2}$$

where $\Delta\mathbf{X} = \mathbf{X}_d - \mathbf{X}_{ref}$; $\mathbf{X}_d$ and $\mathbf{X}_{ref}$ denote the desired and reference trajectories, respectively. $\mathbf{D}_m$, $\mathbf{B}_m$, $\mathbf{K}_m$ are matrices representing impedance behavior. $\mathbf{u}_{imp}$ is generated signal from force regulation and is defined as

$$\mathbf{u}_{imp} = \mathbf{K}_{Pf} \left(\mathbf{F}_{ext} - \mathbf{F}_d\right) + \mathbf{K}_{If} \int \left(\mathbf{F}_{ext} - \mathbf{F}_d\right) \tag{3}$$

where $\mathbf{F}_d \in R^3$ denotes vectors of desired force to be tracked; $\mathbf{K}_{Pf}$ and $\mathbf{K}_{If}$ are 3-by-3 diagonal matrices of proportional and integrated controller gains, respectively.

B. SYSTEM MODELING

The dynamics of the n-DOF serial manipulator is expressed by [52]:

$$\mathbf{M}\left(\mathbf{q}\right)\ddot{\mathbf{q}} + \mathbf{C}\left(\mathbf{q}, \dot{\mathbf{q}}\right)\dot{\mathbf{q}} + \mathbf{G}\left(\mathbf{q}\right) + \boldsymbol{\Delta} + \mathbf{J}^T\left(\mathbf{q}\right)\mathbf{F}_{ext} = \boldsymbol{\tau} \tag{4}$$

where $\mathbf{q}, \dot{\mathbf{q}}, \ddot{\mathbf{q}} \in R^n$ are vectors of joint angle, joint angular velocity, and joint angular acceleration, respectively; $\mathbf{M}\left(\mathbf{q}\right) \in R^{n\times n}$ is the symmetric and positive definite matrix of nominal inertia; $\mathbf{C}\left(\mathbf{q}, \dot{\mathbf{q}}\right) \in R^{n\times n}$ denotes the nominal Coriolis and Centrifugal term matrix; $\mathbf{G}\left(\mathbf{q}\right) \in R^n$ is the nominal gravity term. $\boldsymbol{\tau} \in R^n$ is torque vector acting on the manipulator's joints; $\boldsymbol{\Delta}$ denotes lumped external noise and system modeling error; and $\mathbf{J}\left(\mathbf{q}\right) \in R^{n\times 3}$ is Jacobian matrix from Cartesian space to joint space [12].

Property 1: $\dot{\mathbf{M}}(\mathbf{q}) - 2\mathbf{C}(\mathbf{q}, \dot{\mathbf{q}}) \in R^{n\times n}$ is a skew matrix that satisfies the condition $\mathbf{X}^T[\dot{\mathbf{M}}(\mathbf{q}) - 2\mathbf{C}(\mathbf{q}, \dot{\mathbf{q}})]\mathbf{X} = 0$ for any non-zero vector $\mathbf{X} \in R^n$.

Property 2: The inertia matrix $\mathbf{M}\left(\mathbf{q}\right) \in R^{n\times n}$ is bounded by $m_l \left\|\mathbf{X}\right\|^2 \leq \mathbf{X}^T\mathbf{M}\left(\mathbf{q}\right)\mathbf{X} \leq m^u \left\|\mathbf{X}\right\|^2$, in which m_l and m^u are lower and upper bound positive constants, respectively.

Without losing the generality, let us consider one joint element. Then, the torque acting on one actuator τ_i is calculated by:

$$\tau_i = \begin{cases} A_{ri}(P_{ai1} - P_{ai2}) & \text{(for rotary actuator)} \\ J_{ai}^T\left(q\right)\left(A_{ai1}P_{ai1} - A_{ai2}P_{ai2}\right) & \text{(for cylinder)} \end{cases} \tag{5}$$

where A_{ri}, A_{ai1}, and A_{ai2} are the volumetric area of rotary actuator and areas of piston head part and rod part of the cylinder, respectively; P_{ai1} and P_{ai2} $(i = 1,2,\ldots,n)$ are pressures of two chambers of each actuator; J_{ai} denotes a transform calculation from joint space to actuator space and can be calculated by [12] ($J_{ai} = 1$ in case of the rotary actuator).

It is noteworthy that in case of rotary actuator, $A_{ai1} = A_{ai2} = A_{ri}$. Therefore, A_{ai1} and A_{ai2} are used for calculation in general. The pressures P_{ai1} and P_{ai2} are obtained from the hydraulic continuity equation by:

$$\begin{cases} \dot{P}_{ai1} = \dfrac{\beta}{V_{i1_0} + A_{ai1}x_{ai}} \\ \qquad \times \left[Q_{ai1} - A_{ai1}\dfrac{\partial x_{ai}}{\partial q_i}\dot{q}_i - C_{leak,i}\left(P_{ai1} - P_{ai2}\right)\right] \\ \dot{P}_{ai2} = \dfrac{\beta}{V_{i2_0} - A_{ai2}x_{ai}} \\ \qquad \times \left[-Q_{ai2} + A_{ai2}\dfrac{\partial x_{ai}}{\partial q_i}\dot{q}_i + C_{leak,i}\left(P_{ai1} - P_{ai2}\right)\right] \end{cases} \tag{6}$$

where β is the effective Bulk modulus; $V_{ij_0(j=1,2)}$ are initial volumes of the two chambers; $C_{leak,i}$ is internal leakage coefficient, and $Q_{aij}\left(t\right)$ represents for two flows into and out of the two chambers; x_{ai} is the movement of an actuator, obtained through geometric calculation [12].

Assume that the servo valve dynamics is neglected; then, these supplied flow rates are expressed as

$$\begin{cases} Q_{ai1} = C_d\omega x_{vi}\left(s(x_{vi})\sqrt{\dfrac{2}{\rho}\left(P_s - P_{ai1}\right)}\right. \\ \qquad \left. + s(-x_{vi})\sqrt{\dfrac{2}{\rho}\left(P_{ai1} - P_t\right)}\right) \\ Q_{ai2} = C_d\omega x_{vi}\left(s(x_{vi})\sqrt{\dfrac{2}{\rho}\left(P_{ai2} - P_t\right)}\right. \\ \qquad \left. + s(-x_{vi})\sqrt{\dfrac{2}{\rho}\left(P_s - P_{ai2}\right)}\right) \end{cases} \tag{7}$$

where P_S and P_t are the supply pressure and the returned-to-tank pressure, respectively; C_d is the discharge coefficient, ω is the valve orifice area gradient, ρ is the density of oil, and x_{vi} is the motion of the i^{th} spool of the valve. $s(x_{vi}) = 1$ if $x_{vi} > 0$ and $s(x_{vi}) = 0$ when $x_{vi} \leq 0$ is a function to determine the direction of the spool valve for obtaining flow rate through the proportional servo valve.

C. TOTAL SYSTEM

Define the system state variable as

$$\mathbf{x} = \begin{pmatrix} \mathbf{x_1} & \mathbf{x_2} & \mathbf{x_3} \end{pmatrix}^T = \begin{pmatrix} \mathbf{q} & \dot{\mathbf{q}} & (\mathbf{A}_{a1}\mathbf{P}_{a1} - \mathbf{A}_{a2}\mathbf{P}_{a2}) \end{pmatrix}^T \in R^{3n} \tag{8}$$

where $\mathbf{A}_{a1} = diag\begin{pmatrix} A_{a11} & A_{a21} & \dots & A_{ai1} & \dots & A_{an1} \end{pmatrix} \in R^{n\times n}$ and $\mathbf{A}_{a2} = diag\begin{pmatrix} A_{a12} & A_{a22} & \dots & A_{ai2} & \dots & A_{an2} \end{pmatrix} \in R^{n\times n}$; $\mathbf{P}_{a1} = \begin{pmatrix} P_{a11} & P_{a21} & \dots & P_{ai1} & \dots & P_{an1} \end{pmatrix}^T \in R^n$; $\mathbf{P}_{a2} = \begin{pmatrix} P_{a12} & P_{a22} & \dots & P_{ai2} & \dots & P_{an2} \end{pmatrix}^T \in R^n$.

Then the system behavior under the influence of sensor faults can be obtained. The dynamics of the n-DOF serial hydraulic manipulator including actuators in the constrained framework is finally rewritten as

$$\begin{cases} \dot{\mathbf{x}}_1 = \mathbf{x}_2 \\ \dot{\mathbf{x}}_2 = \mathbf{M}^{-1}(\mathbf{x}_1)(\boldsymbol{\tau} - \mathbf{C}(\mathbf{x}_1, \mathbf{x}_2)\mathbf{x}_2 - \mathbf{G}(\mathbf{x}_1) - \boldsymbol{\Delta}) \\ \quad -\mathbf{M}^{-1}(\mathbf{x}_1)\mathbf{J}^T(\mathbf{q})\mathbf{F}_{ext} \\ \dot{\mathbf{x}}_3 = f(\mathbf{x}_1, \mathbf{x}_2) + \mathbf{g}\mathbf{u} - \boldsymbol{\psi}\mathbf{C}_{leak}(\mathbf{P}_{a1} - \mathbf{P}_{a2}) \\ \mathbf{y} = \mathbf{x}_1 + \mathbf{f}_{ss1} \\ \mathbf{F}_{ext,m} = \mathbf{F}_{ext} + \mathbf{f}_{ss2} \end{cases} \tag{9}$$

where $\mathbf{f}_{ss1} \in R^n$ and $\mathbf{f}_{ss2} \in R^3$ denote the vectors of sensor faults on encoders and force sensor, respectively; $\mathbf{F}_{ext,m} \in R^3$ is a vector of measured interactive force.

The terms $\mathbf{f}$, $\mathbf{g}$, $\boldsymbol{\psi}$ are defined as (10), shown at the bottom of the page.

Assumption 2 ([55]): The system outputs $\mathbf{x}_1$, P_{ai1}, and $P_{ai2}(i = 1, \dots, n)$ are measurable by sensors. Besides, all system states, their first derivative and all system dynamics are continuous and bounded.

Assumption 3: In this scope, to facilitate the proposed control algorithm, the encoder and force sensors are supposed to be faulty. All pressure sensors are fault-free.

Assumption 4 ([55]): All matched uncertainty, (internal leakage), and mismatched uncertainty, (lumped disturbance and external force), and their first derivative are continuous and bounded by pre-determined constants.

Assumption 5: The sensor faults $\mathbf{f}_{ss1}$ and $\mathbf{f}_{ss2}$ are assumed to be slow time-varying in comparison to the system dynamics and bounded, and their time derivative are also assumed to be bounded by positive constants, i.e., $0 \leq \|\mathbf{f}_{ssi}\|_\infty \leq \bar{f}_{ssi}$ and $0 \leq |\dot{\mathbf{f}}_{ssi}| \leq \bar{f}^*_{ssi}$, with $i = 1,2$.

Remark 1: Regarding assumptions 2 and 4, the derivative of the joint angle $\mathbf{x}_1$, i.e., $\mathbf{x}_2$ and the joint angular acceleration, $\dot{\mathbf{x}}_2$, are obtained based on the Levant's differentiator [53]. The estimation of $\mathbf{x}_2$ and $\dot{\mathbf{x}}_2$ can reach the real value with a small estimation error in finite time by choosing suitable values of the estimation gains [54].

Remark 2: Referred to [20], the state observer for $\mathbf{x}_2$ and $\dot{\mathbf{x}}_2$, and the proposed robust FTC scheme can be designed separately. Thereby, the proposed FTC scheme can be constructed with full state feedback being available.

III. FAULT ESTIMATION AND FAULT-TOLERANT CONTROL

In this section, a robust FTC is proposed subject to encoder and force sensors fault. The proposed FTC scheme includes matched/mismatched ESO, PB-IC to regulate the interactive force, a reconfigurable action block, and the main control operator, as shown in FIGURE 2. The ESO is employed to estimate the magnitudes of the sensor faults and the true actual system state for the FTC design. The reconfigurable

$$\begin{aligned} \mathbf{f}(\mathbf{x}_1, \mathbf{x}_2) &\triangleq (f_1(x_{11}, x_{21}), \dots, f_i(x_{1i}, x_{2i}), \dots, f_n(x_{1n}, x_{2n}))^T \in R^n \\ f_i(x_{1i}, x_{2i}) &= \left(-A_{ai1}\frac{\partial x_{ai}}{\partial q_i}\dot{q}_i\psi_{i1} - A_{ai2}\frac{\partial x_{ai}}{\partial q_i}\dot{q}_i\psi_{i2}\right) \\ \psi_{i1} &= \frac{\beta A_{ai1}}{V_{i1_0} + A_{ai1}x_{ai}}, \psi_{i2} = \frac{\beta A_{ai2}}{V_{i2_0} - A_{ai2}x_{ai}} \\ \mathbf{g} &\triangleq diag\begin{pmatrix} g_1 & g_2 & \dots & g_i & \dots & g_n \end{pmatrix} \in R^{n\times n} \\ g_i &= \psi_{1i}\left(s(x_{vi})\sqrt{\frac{2}{\rho}(P_s - P_{ai1})} + s(-x_{vi})\sqrt{\frac{2}{\rho}(P_{ai1} - P_t)}\right)C_d\omega K_{vi} \\ &\quad + \psi_{2i}\left(s(x_{vi})\sqrt{\frac{2}{\rho}(P_{ai2} - P_t)} + s(-x_{vi})\sqrt{\frac{2}{\rho}(P_s - P_{ai2})}\right)C_d\omega K_{vi} \\ \mathbf{C}_{leak} &\triangleq diag\begin{pmatrix} C_{leak,1} & C_{leak,2} & \dots & C_{leak,i} & \dots & C_{leak,n} \end{pmatrix} \in R^{n\times n} \\ \boldsymbol{\psi} &\triangleq diag\begin{pmatrix} \psi_{11} + \psi_{12} & \dots & \psi_{i1} + \psi_{i2} & \dots & \psi_{n1} + \psi_{n2} \end{pmatrix} \in R^{n\times n} \end{aligned} \tag{10}$$

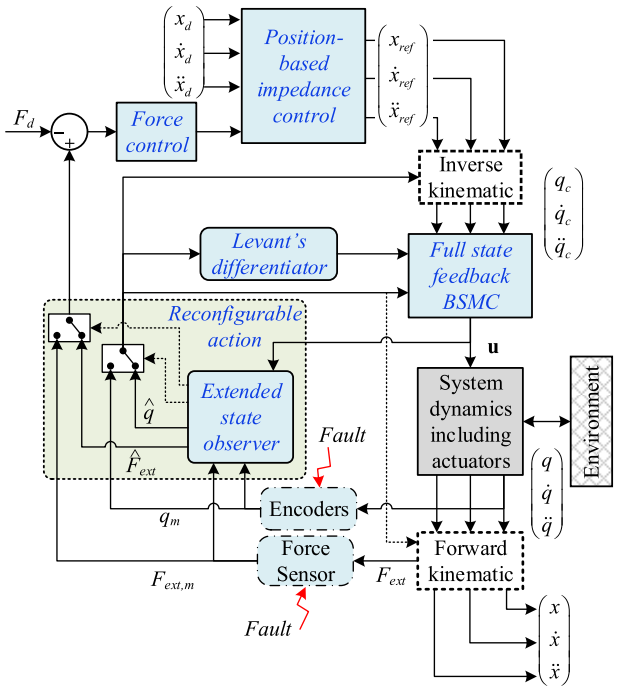

FIGURE 2. Proposed PB-IC-based FTC subject to encoder and force sensor faults.

action block assigns the measured signals from sensors and estimated signals from the ESO as inputs and returns the true value of the system behavior by using a switch. The Levant's differentiator is aimed to obtain unmeasured signal of joint angular velocity for the main controller that is constructed based on full state feedback backstepping sliding mode control (FBSMC) to guarantee the inner loop of position tracking performance. Besides, the system actuator dynamics is also considered in the FBSMC scheme.

A. EXTENDED STATE OBSERVER DESIGN

The sensor faults are considered as extended state variables. Let define $\mathbf{x}_{li} = \psi \mathbf{C}_{leak} (\mathbf{P}_{a1} - \mathbf{P}_{a2})$, $\mathbf{x}_{f_1} = \mathbf{f}_{ss1}$, and $\mathbf{x}_{f_2} = \mathbf{f}_{ss2}$, then the whole system is extended as [56], [57]

$$\begin{cases} \dot{\mathbf{x}}_1 = \mathbf{x}_2 \\ \dot{\mathbf{x}}_2 = \mathbf{M}^{-1}(\mathbf{x}_1)(\boldsymbol{\tau} - \mathbf{C}(\mathbf{x}_1, \mathbf{x}_2)\mathbf{x}_2 - \mathbf{G}(\mathbf{x}_1) - \boldsymbol{\Delta}) \\ -\mathbf{M}^{-1}(\mathbf{x}_1)\mathbf{J}^T(\mathbf{q})\mathbf{F}_{ext} \\ \mathbf{y} = \mathbf{x}_1 + \mathbf{x}_{f_1} \\ \dot{\mathbf{x}}_{f_1} = \mathbf{h}_1(t) \\ \mathbf{F}_{ext,m} = \mathbf{F}_{ext} + \mathbf{x}_{f_2} \\ \dot{\mathbf{x}}_{f_2} = \mathbf{h}_2(t) \end{cases} \tag{11}$$

$$\begin{cases} \dot{\mathbf{x}}_3 = f(\mathbf{x}_1, \mathbf{x}_2) + \mathbf{g}\mathbf{u} - \mathbf{x}_{li} \\ \dot{\mathbf{x}}_{li} = \mathbf{h}(t) \end{cases} \tag{12}$$

where $\mathbf{h}(t) \in R^n$, $\mathbf{h}_1(t) \in R^n$, and $\mathbf{h}_2(t) \in R^3$ are vectors corresponding to the derivative of the internal leakage and sensor faults (encoders and force sensors), respectively.

Under the influence of the sensor faults, the robust observer based on ESO is designed to estimate the system state as

$$\begin{cases} \dot{\hat{\mathbf{x}}}_1 = \hat{\mathbf{x}}_2 - \dfrac{\boldsymbol{\alpha}_1}{\sigma_1}(\hat{\mathbf{y}} - \mathbf{y}) \\ \dot{\hat{\mathbf{x}}}_2 = \mathbf{M}^{-1}(\mathbf{x}_1)(\boldsymbol{\tau} - \mathbf{C}(\mathbf{x}_1, \mathbf{x}_2)\mathbf{x}_2 - \mathbf{G}(\mathbf{x}_1) - \boldsymbol{\Delta}) \\ -\mathbf{M}^{-1}(\mathbf{x}_1)\mathbf{J}^T(\mathbf{q})\hat{\mathbf{F}}_{ext} - \dfrac{\boldsymbol{\alpha}_2}{\sigma_1^2}(\hat{\mathbf{y}} - \mathbf{y}) \\ \hat{\mathbf{y}} = \hat{\mathbf{x}}_1 + \hat{\mathbf{x}}_{f_1} - \dfrac{\boldsymbol{\eta}_{f1}}{\sigma_1}(\hat{\mathbf{y}} - \mathbf{y}) \\ \dot{\hat{\mathbf{x}}}_{f_1} = -\dfrac{\boldsymbol{\eta}_{f1}}{\sigma_1^3}(\hat{\mathbf{y}} - \mathbf{y}) \\ \hat{\mathbf{F}}_{ext,m} = K_e\left(\hat{\mathbf{X}}_a - \mathbf{X}_e\right) + \hat{\mathbf{x}}_{f_2} \\ \dot{\hat{\mathbf{x}}}_{f_2} = -\dfrac{\boldsymbol{\eta}_{f2}}{\sigma_1^3}\left(\hat{\mathbf{F}}_{ext,m} - \mathbf{F}_{ext,m}\right) \end{cases} \tag{13}$$

$$\begin{cases} \dot{\hat{\mathbf{x}}}_3 = \mathbf{f}(\mathbf{x}_1, \mathbf{x}_2) + \mathbf{g}\mathbf{u} - \hat{\mathbf{x}}_{li} - \dfrac{2\boldsymbol{\alpha}_3}{\sigma_2}(\hat{\mathbf{x}}_3 - \mathbf{x}_3) \\ \dot{\hat{\mathbf{x}}}_{li} = -\dfrac{\boldsymbol{\alpha}_3}{\sigma_2^2}(\hat{\mathbf{x}}_3 - \mathbf{x}_3) \end{cases} \tag{14}$$

where $\hat{\mathbf{x}}_i$ is the estimate of system state $\mathbf{x}_i$ (i = 1,2,3); $\hat{\mathbf{F}}_{ext,m}$ is the estimate of measured interactive force $\mathbf{F}_{ext,m}$; and $\hat{\mathbf{x}}_{f_j}$, with $(j = 1,2)$, denotes the estimate of real sensor fault $\mathbf{x}_{f_j}$; $\boldsymbol{\alpha}_1$, $\boldsymbol{\alpha}_2$, $\boldsymbol{\alpha}_3$, $\boldsymbol{\eta}_{f1}$ are n-by-n tuned diagonal matrices gains of the ESO; $\boldsymbol{\eta}_{f2} \in R^3$ is diagonal matrix; σ_1 and σ_2 are arbitrarily small relating the bandwidth of the ESO.

The calculation of the end-effector estimation $\hat{\mathbf{X}}_a$ is calculated from the system state $\hat{\mathbf{x}}_1$ through forward kinematic as

$$\hat{\mathbf{X}}_a = \mathbf{f}(\hat{\mathbf{x}}_1) \tag{15}$$

where $\mathbf{f}(\hat{\mathbf{x}}_1) : R^n \rightarrow R^3$ denotes the forward kinematic calculation.

From (11) to (14), the dynamics of the state estimation errors is given by:

$$\begin{cases} \dot{\tilde{\mathbf{x}}}_1 = \tilde{\mathbf{x}}_2 - \dfrac{\boldsymbol{\alpha}_1}{\sigma_1}\tilde{\mathbf{y}} \\ \dot{\tilde{\mathbf{x}}}_2 = -\mathbf{M}^{-1}(\mathbf{x}_1)\left(\mathbf{J}^T(\mathbf{x}_1)K_e\mathbf{f}(\tilde{\mathbf{x}}_1) - \tilde{\mathbf{x}}_{f2}\right) - \dfrac{\boldsymbol{\alpha}_2}{\sigma_1^2}\tilde{\mathbf{y}} \\ \tilde{\mathbf{y}} = \tilde{\mathbf{x}}_1 + \tilde{\mathbf{x}}_{f_1} - \dfrac{\boldsymbol{\eta}_{f1}}{\sigma_1}\tilde{\mathbf{y}} \\ \dot{\tilde{\mathbf{x}}}_{f_1} = -\dfrac{\boldsymbol{\eta}_{f1}}{\sigma_1^3}\tilde{\mathbf{y}} + \mathbf{h}_1 \\ \tilde{\mathbf{F}}_{ext,m} = K_e\mathbf{f}(\tilde{\mathbf{x}}_1) + \tilde{\mathbf{x}}_{f_2} \\ \dot{\tilde{\mathbf{x}}}_{f_2} = -\dfrac{\boldsymbol{\eta}_{f2}}{\sigma_1^3}\left(K_e\mathbf{f}(\tilde{\mathbf{x}}_1) + \tilde{\mathbf{x}}_{f_2}\right) + \mathbf{h}_2 \end{cases} \tag{16}$$

$$\begin{cases} \dot{\tilde{\mathbf{x}}}_3 = -\tilde{\mathbf{x}}_{li} - \dfrac{2\boldsymbol{\alpha}_3}{\sigma_2}\tilde{\mathbf{x}}_3 \\ \dot{\tilde{\mathbf{x}}}_{li} = -\dfrac{\boldsymbol{\alpha}_3^2}{\sigma_2^2}\tilde{\mathbf{x}}_3 + \mathbf{h} \end{cases} \tag{17}$$

where $(\tilde{\bullet}) = (\bullet) - (\hat{\bullet})$, $\mathbf{f}(\tilde{\mathbf{x}}_1) = \hat{\mathbf{X}}_a - \mathbf{X}_a \in R^3$.

Assumption 6: The nonlinear term $\mathbf{f}(\tilde{\mathbf{x}}_1)$ has a Lipchitz of $\mathbf{f}_{fk}\tilde{\mathbf{x}}_1$. It is noteworthy from (16) that the matrix of the state estimation error of the end-effector position, $\mathbf{f}(\tilde{\mathbf{x}}_1)$, depending on the estimation error of the joint angle, should be obtained from forward kinematic calculation. However, because it is the function of joint angle error and is bounded by $\mathbf{f}_{fk}\tilde{\mathbf{x}}_1$, the estimation error of the forward kinematic is linearized around the equilibrium of zero and thus, in this scope, it is simplified by using a constant matrix gain $\mathbf{f}_{fk} \in R^{3\times n}$, i.e., $\mathbf{f}(\tilde{\mathbf{x}}_1) \approx \mathbf{f}_{fk}\tilde{\mathbf{x}}_1$. Moreover, neglecting the system dynamics error and identification process, it can be mathematically obtained without any other estimated error generated.

From the third equation of (16), one obtains:

$$\tilde{\mathbf{y}} = \left(\mathbf{I}_n + \frac{1}{\sigma_1}\boldsymbol{\eta}_{f1}\right)^{-1}\left(\tilde{\mathbf{x}}_1 + \tilde{\mathbf{x}}_{f_1}\right) \tag{18}$$

Then, the dynamics of the state estimation error becomes:

$$\begin{cases} \dot{\tilde{\mathbf{x}}}_1 = \dfrac{1}{\sigma_1}\left(-\boldsymbol{\Xi}_{11}\tilde{\mathbf{x}}_1 + \tilde{\mathbf{x}}_2 - \boldsymbol{\Xi}_{13}\tilde{\mathbf{x}}_{f_1}\right) \\ \sigma_1\dot{\tilde{\mathbf{x}}}_2 = \dfrac{1}{\sigma_1}\left(-\boldsymbol{\Xi}_{21}\tilde{\mathbf{x}}_1 - \boldsymbol{\Xi}_{23}\tilde{\mathbf{x}}_{f_1} - \boldsymbol{\Xi}_{24}\tilde{\mathbf{x}}_{f_2}\right) \\ \sigma_1^2\dot{\tilde{\mathbf{x}}}_{f_1} = \dfrac{1}{\sigma_1}\left(-\boldsymbol{\Xi}_{31}\tilde{\mathbf{x}}_1 - \boldsymbol{\Xi}_{33}\tilde{\mathbf{x}}_{f_1}\right) + \varepsilon_1^2\mathbf{h}_1 \\ \sigma_1^2\dot{\tilde{\mathbf{x}}}_{f_2} = \dfrac{1}{\sigma_1}\left(-\boldsymbol{\Xi}_{41}\tilde{\mathbf{x}}_1 - \boldsymbol{\Xi}_{44}\tilde{\mathbf{x}}_{f_2}\right) + \varepsilon_1^2\mathbf{h}_2 \end{cases} \tag{19}$$

$$\begin{cases} \dot{\tilde{\mathbf{x}}}_3 = -\dfrac{2\boldsymbol{\alpha}_3}{\sigma_2}\tilde{\mathbf{x}}_3 - \tilde{\mathbf{x}}_{li} \\ \sigma_2\dot{\tilde{\mathbf{x}}}_{li} = -\dfrac{\boldsymbol{\alpha}_3^2}{\sigma_2}\tilde{\mathbf{x}}_3 + \sigma_2\mathbf{h} \end{cases} \tag{20}$$

where $\boldsymbol{\Xi}_{11} = \boldsymbol{\alpha}_2\left(\mathbf{I}_n + \frac{1}{\sigma_1}\boldsymbol{\eta}_{f1}\right) \in R^{n\times n}$, $\boldsymbol{\Xi}_{13} = \boldsymbol{\Xi}_{11} \in R^{n\times n}$, $\boldsymbol{\Xi}_{21} = \sigma_1^2\mathbf{M}^{-1}K_e\mathbf{f}_{fk} + \boldsymbol{\alpha}_2\left(\mathbf{I}_n + \frac{1}{\sigma_1}\boldsymbol{\eta}_{f1}\right) \in R^{n\times n}$, $\boldsymbol{\Xi}_{23} = \boldsymbol{\alpha}_2\left(\mathbf{I}_n + \frac{1}{\sigma_1}\boldsymbol{\eta}_{f1}\right) \in R^{n\times n}$, $\boldsymbol{\Xi}_{24} = \mathbf{M}^{-1} \in R^{n\times 3}$, $\boldsymbol{\Xi}_{31} = \boldsymbol{\eta}_{f1} \in R^{n\times n}$, $\boldsymbol{\Xi}_{33} = \boldsymbol{\Xi}_{31} \in R^{n\times n}$, $\boldsymbol{\Xi}_{41} = \mathbf{f}_{fk}\boldsymbol{\eta}_{f2}K_e \in R^{3\times n}$, $\boldsymbol{\Xi}_{44} = \boldsymbol{\eta}_{f2} \in R^{3\times 3}$.

Define auxiliary vectors of estimated error $\boldsymbol{\varepsilon}_1$ and $\boldsymbol{\varepsilon}_2$ as

$$\boldsymbol{\varepsilon}_1 = \left(\tilde{\mathbf{x}}_1, \sigma_1\tilde{\mathbf{x}}_2, \sigma_1^2\tilde{\mathbf{x}}_{f1}, \sigma_1^2\tilde{\mathbf{x}}_{f2}\right)^T \in R^{3n+3} \tag{21}$$

$$\boldsymbol{\varepsilon}_2 = \left(\tilde{\mathbf{x}}_3, \sigma_2\tilde{\mathbf{x}}_{li}\right)^T \in R^{2n} \tag{22}$$

Then, the dynamics state estimation errors become:

$$\dot{\boldsymbol{\varepsilon}}_1 = \frac{1}{\sigma_1}\mathbf{A}_1\boldsymbol{\varepsilon}_1 + \sigma_1^2\mathbf{B}_1\mathbf{H}_1 \tag{23}$$

$$\dot{\boldsymbol{\varepsilon}}_2 = \frac{1}{\sigma_2}\mathbf{A}_2\boldsymbol{\varepsilon}_2 + \sigma_2\mathbf{B}_2\mathbf{H}_2 \tag{24}$$

with

$$\mathbf{A}_1 = \begin{bmatrix} -\boldsymbol{\Xi}_{11} & \mathbf{I}_n & -\boldsymbol{\Xi}_{13} & \mathbf{0}_{n\times 3} \\ -\boldsymbol{\Xi}_{21} & \mathbf{0}_{n\times n} & -\boldsymbol{\Xi}_{23} & -\boldsymbol{\Xi}_{24} \\ -\boldsymbol{\Xi}_{31} & \mathbf{0}_{n\times n} & -\boldsymbol{\Xi}_{33} & \mathbf{0}_{n\times 3} \\ -\boldsymbol{\Xi}_{41} & \mathbf{0}_{3\times n} & \mathbf{0}_{3\times n} & -\boldsymbol{\Xi}_{44} \end{bmatrix} \in R^{(3n+3)\times(3n+3)},$$

$$\mathbf{A}_2 = \begin{bmatrix} -2\boldsymbol{\alpha}_3 & -\mathbf{I}_{n\times n} \\ -\boldsymbol{\alpha}_3 & \mathbf{0}_{n\times n} \end{bmatrix} \in R^{2n\times 2n},$$

$$\begin{aligned} \mathbf{B}_2 &= diag\begin{pmatrix}\mathbf{I}_n & \mathbf{I}_n\end{pmatrix} \in R^{2n\times 2n}, \\ \mathbf{B}_1 &= diag\begin{pmatrix}\mathbf{I}_n & \mathbf{I}_n & \mathbf{I}_n & \mathbf{I}_3\end{pmatrix} \in R^{(3n+3)\times(3n+3)}, \\ \mathbf{H}_1 &= \begin{pmatrix}\mathbf{0}_{n\times 1} & \mathbf{0}_{n\times 1} & \mathbf{h}_1 & \mathbf{h}_2\end{pmatrix} \in R^{3n+3}, \\ \mathbf{H}_2 &= \begin{pmatrix}\mathbf{0}_{n\times 1} & \mathbf{h}\end{pmatrix} \in R^{2n} \end{aligned} \tag{25}$$

where $\mathbf{I}_{n\times n}$ denotes n-by-n identity matrix, $\mathbf{0}_{p\times q}$ denotes p-by-q zero matrix.

The matrices $\mathbf{A}_1$ and $\mathbf{A}_2$ are Hurwitz, then there exist matrices $\mathbf{P}_1 \in R^{(3n+3)\times(3n+3)}$ and $\mathbf{P}_2 \in R^{2n\times 2n}$ that satisfy:

$$\begin{cases} \mathbf{A}_1^T\mathbf{P}_1 + \mathbf{P}_1\mathbf{A}_1 = -\mathbf{I}_{3n+3} \\ \mathbf{A}_2^T\mathbf{P}_2 + \mathbf{P}_2\mathbf{A}_2 = -\mathbf{I}_{2n} \end{cases} \tag{26}$$

Theorem 1: Consider the faulty system (11), and the proposed robust observer based on the ESO in (13), and Assumption 5, all signals of the system are uniformly ultimately bounded (UUB) and converges to the small neighborhood of the origin.

Proof of Theorem 1: See Appendix.

Theorem 2: Consider the system (12), and the ESO in (14), and Assumptions 4 and 5, all signals of this system are UUB and converges to the small neighborhood of the origin.

Proof of Theorem 2: See Appendix.

B. FAULT-TOLERANT CONTROL DESIGN

In order to address the influence of sensor faults and matched uncertainty, the FTC-based FBSMC is step-by-step designed.

Step 1: Define the tracking error $\mathbf{e}_1 = \mathbf{x}_1 - \mathbf{x}_{1d} \in R^n$ and, $\mathbf{e}_2 = \dot{\mathbf{e}}_1 = \mathbf{x}_2 - \mathbf{x}_{2d} \in R^n$ where $\mathbf{x}_{1d}, \mathbf{x}_{2d} \in R^n$ are the vector of desired angles and angular velocities, respectively. Then, the sliding surface is chosen as

$$\mathbf{s}_1 = \mathbf{e}_2 + \lambda\mathbf{e}_1 \tag{27}$$

where $\boldsymbol{\lambda} \triangleq diag\begin{pmatrix}\lambda_1 & \lambda_2 & \ldots & \lambda_i & \ldots & \lambda_n\end{pmatrix} \in R^{n\times n}$ is the positive definite matrix.

According to [12], the following auxiliary variable is utilized:

$$\begin{cases} \mathbf{x}_{2s} = \mathbf{x}_2 - \mathbf{s}_1 = \mathbf{x}_{2d} - \lambda\mathbf{e}_1 \in R^n \\ \dot{\mathbf{x}}_{2s} = \dot{\mathbf{x}}_2 - \dot{\mathbf{s}}_1 = \dot{\mathbf{x}}_{2d} - \lambda\mathbf{e}_2 \in R^n \end{cases} \tag{28}$$

In order to cancel out the influence of mismatched uncertainties, the following adaptive law is presented:

$$\dot{\hat{\boldsymbol{\Delta}}} = -\mathbf{s}_1 \tag{29}$$

Then, a virtual torque command is designed as

$$\begin{aligned} \mathbf{x}_{3d} = \mathbf{M}(\mathbf{x}_1)\dot{\mathbf{x}}_{2s} + \mathbf{C}(\mathbf{x}_1, \mathbf{x}_2)\mathbf{x}_{2s} + \mathbf{G}(\mathbf{x}_1) + \mathbf{J}^T\hat{\mathbf{F}}_{ext} + \hat{\boldsymbol{\Delta}} \\ - \mathbf{K}_1\mathbf{s}_1 - \boldsymbol{\eta}_1\tanh\left(\frac{\mathbf{s}_1}{\delta}\right) \end{aligned} \tag{30}$$

where $\mathbf{K}_1 = diag\begin{pmatrix}K_{11} & K_{12} & \ldots & K_{1i} & \ldots & K_{1n}\end{pmatrix} \in R^{n\times n}$ and $\boldsymbol{\eta}_1 = diag\begin{pmatrix}\eta_{11} & \eta_{12} & \ldots & \eta_{1i} & \ldots & \eta_{1n}\end{pmatrix} \in R^{n\times n}$ are positive definite matrices, in which the term $-\mathbf{K}_1\mathbf{s}_1$ is added to enhance the convergence rate when $\mathbf{s}_1$ is large; and δ is arbitrarily small.

Remark 3: The term $\boldsymbol{\eta}_1 \tanh\left(\mathbf{s}_1/\delta\right)$ is employed instead of using signum function, i.e., $\boldsymbol{\eta}_1 sign\left(\mathbf{s}_1\right)$ because this discontinuous function is un-differentiable, and a vector $\tanh\left(\mathbf{s}_1/\delta\right) = \left(\tanh\left(s_{11}/\delta\right);\ \tanh\left(s_{12}/\delta\right);\ \ldots\ ;\ \tanh\left(s_{1n}/\delta\right)\right)$ is a column vector with s_{1i} is the sliding surface of joint i^{th}.

Step 2: Define the actuator torque tracking error $\mathbf{s}_2 = \mathbf{x}_3 - \mathbf{x}_{3d} \in R^n$. Hence, the control input signal is designed as

$$\mathbf{u}_v = \mathbf{g}^{-1}\left(-\mathbf{f}\left(\mathbf{x}_1, \mathbf{x}_2\right) - \hat{\mathbf{x}}_{li} + \dot{\mathbf{x}}_{3d} - \mathbf{K}_2\mathbf{s}_2 - \boldsymbol{\eta}_2 sign\left(\mathbf{s}_2\right) - \mathbf{J}_a^T\mathbf{s}_1\right) \tag{31}$$

where $\mathbf{K}_2 = diag\left(K_{21}\ K_{22}\ \ldots\ K_{2i}\ \ldots\ K_{2n}\right) \in R^{n\times n}$ and $\boldsymbol{\eta}_2 = diag\left(\eta_{21}\ \eta_{22}\ \ldots\ \eta_{2i}\ \ldots\ \eta_{2n}\right) \in R^{n\times n}$ are positive definite matrices, in which the term $-\mathbf{K}_2\mathbf{s}_2$ is added to enhance the convergence rate when $\mathbf{s}_2$ is large, and $sign\left(\mathbf{s}_2\right) = \left(sign\left(s_{21}\right)\ sign\left(s_{22}\right)\ \ldots\ sign\left(s_{2n}\right)\right)^T \in R^n$.

Remark 4: Regarding the virtual control law in (30), it is noteworthy that in free-motion, there is no interactive force $\mathbf{F}_{ext}$. The external force disturbance in this case is presented by lumped uncertainty Δ, including noise or other external disturbances and modeling error. In case of constrained motion, the interactive force dominates the influence of Δ, then the measured force (in case of fault-free) or force estimation can be approximated as equal as the actual interactive force.

IV. CLOSED-LOOP SYSTEM ANALYSIS

Theorem 3: Consider the system dynamics (9), with the use of the fault estimation algorithm (13), matched disturbance observer (14) based on ESO, control laws (30) and (31), and Assumptions 4 and 5, the system stability is guaranteed and the system tracking performance is maintained in good condition under the presence of sensor faults and matched uncertainty.

Proof of theorem 3:

Consider the Lyapunov candidate as

$$V = \frac{1}{2}\mathbf{s}_1^T\mathbf{M}\mathbf{s}_1 + \frac{1}{2}\mathbf{s}_2^T\mathbf{s}_2 + \frac{1}{2}\tilde{\boldsymbol{\Delta}}^T\tilde{\boldsymbol{\Delta}} + \frac{1}{2}\boldsymbol{\varepsilon}_1^T\mathbf{P}_1\boldsymbol{\varepsilon}_1 + \frac{1}{2}\boldsymbol{\varepsilon}_2^T\mathbf{P}_2\boldsymbol{\varepsilon}_2 \tag{32}$$

Taking derivative the Lyapunov candidate V yields:

$$\begin{aligned}\dot{V} = &-\mathbf{s}_1^T\left(\mathbf{x}_3 - \mathbf{M}\left(\mathbf{x}_1\right)\dot{\mathbf{x}}_{2s} - \mathbf{C}\left(\mathbf{x}_1, \mathbf{x}_2\right)\mathbf{x}_{2s} - \mathbf{G}\left(\mathbf{x}_1\right)\right)\\ &- \mathbf{s}_1^T\mathbf{J}^T\left(\mathbf{x}_1\right)\mathbf{F}_{ext} + \mathbf{s}_1^T\left(\tilde{\boldsymbol{\Delta}} + \hat{\boldsymbol{\Delta}}\right) + \dot{\tilde{\boldsymbol{\Delta}}}^T\tilde{\boldsymbol{\Delta}}\\ &+ \mathbf{s}_2^T\left(\mathbf{f}\left(\mathbf{x}_1, \mathbf{x}_2\right) + \mathbf{g}\mathbf{u} + \mathbf{x}_{li} - \mathbf{x}_{3d}\right)\\ &- \frac{1}{2\sigma_1}\boldsymbol{\varepsilon}_1^T\mathbf{I}_{4n}\boldsymbol{\varepsilon}_1 + \sigma_1^2\boldsymbol{\varepsilon}_1^T\mathbf{P}_1\mathbf{B}_1\mathbf{H}_1\\ &- \frac{1}{2\sigma_2}\boldsymbol{\varepsilon}_2^T\mathbf{I}_{2n}\boldsymbol{\varepsilon}_2 + \sigma_2\boldsymbol{\varepsilon}_2^T\mathbf{P}_2\mathbf{B}_2\mathbf{H}_2\end{aligned} \tag{33}$$

By using the adaptive law (29), virtual torque command (30), and the control signal (31), the influence of the lumped mismatched uncertainty is canceled out. Then, the derivative of the Lyapunov V becomes:

$$\begin{aligned}\dot{V} = &-\sum_{i=1}^{2}\mathbf{s}_i^T\mathbf{K}_i\mathbf{s}_i - \mathbf{s}_1^T\left(\boldsymbol{\eta}_1\tanh\left(\frac{\mathbf{s}_1}{\delta}\right) - \tilde{\mathbf{F}}_{ext}\right)\\ &- \mathbf{s}_2^T\left(\boldsymbol{\eta}_2 sign\left(\mathbf{s}_2\right) - \tilde{\mathbf{x}}_{li}\right)\\ &- \frac{1}{2\sigma_1}\boldsymbol{\varepsilon}_1^T\mathbf{I}_{3n+3}\boldsymbol{\varepsilon}_1 + \sigma_1^2\boldsymbol{\varepsilon}_1^T\mathbf{P}_1\mathbf{B}_1\mathbf{H}_1\\ &- \frac{1}{2\sigma_2}\boldsymbol{\varepsilon}_2^T\mathbf{I}_{2n}\boldsymbol{\varepsilon}_2 + \sigma_2\boldsymbol{\varepsilon}_2^T\mathbf{P}_2\mathbf{B}_2\mathbf{H}_2\end{aligned} \tag{34}$$

Apply Young's inequality, the derivative of the Lyapunov candidate is obtained as

$$\begin{aligned}\dot{V} \le &-\mathbf{s}_1^T\mathbf{K}_1\mathbf{s}_1 - \mathbf{s}_2^T\mathbf{K}_2\mathbf{s}_2\\ &- \mathbf{s}_1^T\left(\boldsymbol{\eta}_1\tanh\left(\frac{\mathbf{s}_1}{\delta}\right) - \tilde{\mathbf{F}}_{ext}\right) - \mathbf{s}_2^T\left(\boldsymbol{\eta}_2 sign\left(\mathbf{s}_1\right) - \tilde{\mathbf{x}}_{li}\right)\\ &- \frac{1}{2}\left(\frac{1}{\sigma_1} - \sigma_1^2\lambda_{\max}\left(\mathbf{P}_1^T\mathbf{B}_1\mathbf{B}_1^T\mathbf{P}_1\right)\right)\|\boldsymbol{\varepsilon}_1\|^2\\ &+ \frac{1}{2}\sigma_1^2\mathbf{H}_1^T\mathbf{H}_1\\ &- \frac{1}{2}\left(\frac{1}{\sigma_2} - \sigma_2\lambda_{\max}\left(\mathbf{P}_2^T\mathbf{B}_2\mathbf{B}_2^T\mathbf{P}_2\right)\right)\|\boldsymbol{\varepsilon}_2\|^2\\ &+ \frac{1}{2}\sigma_2\mathbf{H}_2^T\mathbf{H}_2\end{aligned} \tag{35}$$

$$\Leftrightarrow \dot{V} \le -\gamma V + \zeta \tag{36}$$

where

$$\begin{aligned}\gamma = &\min\begin{pmatrix}\frac{1}{\sigma_1} - \sigma_1^2\lambda_{\max}\left(\mathbf{P}_1^T\mathbf{B}_1\mathbf{B}_1^T\mathbf{P}_1\right),\\ \frac{1}{\sigma_2} - \sigma_2^2\lambda_{\max}\left(\mathbf{P}_2^T\mathbf{B}_2\mathbf{B}_2^T\mathbf{P}_2\right),\\ \lambda_{\min}\left(\mathbf{K}_1\right), \lambda_{\min}\left(\mathbf{K}_2\right), \lambda_{\min}\left(\boldsymbol{\eta}_1\right), \lambda_{\min}\left(\boldsymbol{\eta}_2\right)\end{pmatrix}\\ &\ge 0,\\ \zeta = &\mathbf{s}_1^T\tilde{\mathbf{F}}_{ext} + \mathbf{s}_2^T\tilde{\mathbf{x}}_{li} + \frac{1}{2}\sigma_1^2\mathbf{H}_1^T\mathbf{H}_1 + \frac{1}{2}\sigma_2\mathbf{H}_2^T\mathbf{H}_2.\end{aligned}$$

Remark 5: Based on assumption 4, the estimated errors of matched and mismatched uncertainties are bounded by assumedly predetermined upper bound, i.e., $\|\tilde{\cdot}\|^2 \le \bar{\delta}_{bound}$. Hence, the robust terms $\boldsymbol{\eta}_i$ should be designed such that $\eta_{ij(i=1,2;j=1,..,n)} \ge \bar{\delta}_{bound}$.

According to [49] and [58], it can be concluded that the proposed algorithm is UUB with an exponential convergence rate γ in the presence of mismatched external force interaction, sensor faults and matched uncertainty (i.e. internal leakage). As a result, the Lyapunov candidate V is bounded by:

$$V \le V\left(0\right)e^{-\gamma t} + \frac{\zeta}{\gamma}\left(1 - e^{-\gamma t}\right) \tag{37}$$

Remark 6: In order to enhance the force estimation, the estimation algorithm (13) is modified with adding signum

function by:

$$\begin{cases} \dot{\hat{\mathbf{x}}}_1 = \hat{\mathbf{x}}_2 - \dfrac{\alpha_1}{\sigma_1}\left(\hat{\mathbf{y}} - \mathbf{y}\right) \\ \dot{\mathbf{x}}_2 = \mathbf{M}^{-1}\left(\mathbf{x}_1\right)\left(\boldsymbol{\tau} - \mathbf{C}\left(\mathbf{x}_1, \mathbf{x}_2\right)\mathbf{x}_2 - \mathbf{G}\left(\mathbf{x}_1\right) - \boldsymbol{\Delta}\right) \\ -\mathbf{M}^{-1}\left(\mathbf{x}_1\right)\mathbf{J}^T\left(\mathbf{q}\right)\hat{\mathbf{F}}_{ext} - \dfrac{\alpha_2}{\sigma_1^2}\left(\hat{\mathbf{y}} - \mathbf{y}\right) \\ \hat{\mathbf{y}} = \hat{\mathbf{x}}_1 + \hat{\mathbf{x}}_{f_1} - \dfrac{\eta_{f1}}{\sigma_1}\left(\hat{\mathbf{y}} - \mathbf{y}\right) \\ \dot{\mathbf{x}}_{f_1} = -\dfrac{\eta_{f1}}{\sigma_1^3}\left(\hat{\mathbf{y}} - \mathbf{y}\right) \\ \hat{\mathbf{F}}_{ext,m} = K_e\left(\hat{\mathbf{X}}_a - \mathbf{X}_e\right) + \hat{\mathbf{x}}_{f_2} \\ \dot{\hat{\mathbf{x}}}_{f_2} = -\dfrac{\eta_{f2}}{\sigma_1^3}\left(\hat{\mathbf{F}}_{ext,m} - \mathbf{F}_{ext,m}\right) \\ -\dfrac{\eta_{f3}}{\sigma_1^3} sign\left(\hat{\mathbf{F}}_{ext,m} - \mathbf{F}_{ext,m}\right) \end{cases} \tag{38}$$

where $\boldsymbol{\eta}_{f3} \in R^3$ is a diagonal positive definite matrix.

V. NUMERICAL SIMULATION

A. SETUP SCENARIO

In this section, the scenario in which the influence of encoder and force sensor faults and effectiveness of the proposed FTC based on the integration of the FBSMC with ESO is verified through several comparative simulations on a 3-DOF serial hydraulic manipulator (n = 3), as shown in FIGURE 3 [12]. In order to simplify the calculation, the first joint of the 3-DOF serial hydraulic manipulator is fixed, i.e. $\mathbf{q}_1 = \dot{\mathbf{q}}_1 = 0$. Then, the objective is to investigate the behavior of the 2-DOF serial manipulator (n = 2) subjects to encoder and force sensor faults. The constrained framework is located in the plane S_Z that is parallel to the plane (XOY). The system parameters, including mechanical part and hydraulic actuator part, are given in TABLE 1 and TABLE 2, respectively. The FBSMC controller gains are $\boldsymbol{\lambda} = 1000\mathbf{I}_2$, $\mathbf{K}_1 = 120\mathbf{I}_2$, $\boldsymbol{\eta}_1 = 0.5\mathbf{I}_2$, $\delta = 10^{-4}$, $\mathbf{K}_2 = 120\mathbf{I}_2$, $\boldsymbol{\eta}_2 = 0.5\mathbf{I}_2$.

B. SIMULATION RESULTS

1) CASE STUDY 1

In the first case study, we verify the effectiveness of the proposed fault estimation in the case of only signal faults occurrence on joint angle encoders in free motion. The desired joint trajectory and fault signals are given by:

$$\mathbf{q}_d = \mathbf{x}_{1d} = \begin{pmatrix} 0 \\ 45 + 30\sin\left(\dfrac{2\pi}{5}t\right) \\ 45 + 30\sin\left(\dfrac{2\pi}{5}t + \dfrac{\pi}{4}\right) \end{pmatrix} \tag{39}$$

$$\mathbf{f}_{ss1} = \begin{pmatrix} f_{ss1,\text{joint2}} & f_{ss1,\text{joint3}} \end{pmatrix}^T,$$

$$\begin{cases} f_{ss1,\text{joint2}} = \begin{cases} 0 & \text{(degree) if } t < 10s \\ 10 & \text{(degree) if } t \geq 10s \end{cases} \\ f_{ss1,\text{joint3}} = \begin{cases} 0 & \text{(degree) if } t < 20s \\ 10 & \text{(degree) if } t \geq 20s \end{cases} \end{cases} \tag{40}$$

The observer gains in (13) are $\sigma_1 = 0.1$, $\boldsymbol{\alpha}_1 = 2\mathbf{I}_2$, $\boldsymbol{\alpha}_2 = 2\mathbf{I}_2$, $\boldsymbol{\eta}_{f1} = 4\mathbf{I}_2$. The values of system performance and observers are all initialized as zero.

The idea of the robust observer is that the measured joint angle, including real and faulty signals, is estimated; thereby, the actual joint angle and faulty signal are then estimated and feedback to the controller. The position tracking performance and state estimation of the two joints are depicted in FIGURE 4. The black continuous line denotes the desired joint angle trajectory $q_{i,ref}$, the blue dash line denotes the measured joint angles $q_{i,m}$, the red dot-dash

TABLE 1. Mechanical parameters [20].

Symbol	Quantity	Value
m_1	Mass of the first link	2 [kg]
m_2	Mass of the second link	5.1 [kg]
m_3	Mass of the third link	4.7 [kg]
L_1	Length of the second link	0.5 [m]
L_2	Length of the third link	0.2 [m]

TABLE 2. Hydraulic parameters [20].

Symbol	Quantity	Value [unit]
P_S	Supply pressure from the tank	100 [bar]
P_t	Return pressure to the tank	1 [bar]
K_v	Gain factor of the valve dynamics	$1.2\text{x}10^{-3}$ [m/V]
ω	Servo valve area gradient	0.024 [m^2]
ρ	Oil density	800 [kg/m^3]
β	Effective Bulk modulus	$1.25\text{x}10^{9}$ [pa]
A_{11}, A_{12}	Volumetric area of rotary actuator 2	$2\text{x}10^{-4}$ [m^3/rad]
A_{21}, A_{22}	Volumetric area of rotary actuator 3	$1.2\text{x}10^{-4}$ [m^3/rad]
A_{31}	Cylinder area of piston head part	$1.53\text{x}10^{-3}$ [m^2]
A_{32}	Cylinder area of piston rod part	$1.04\text{x}10^{-3}$ [m^2]

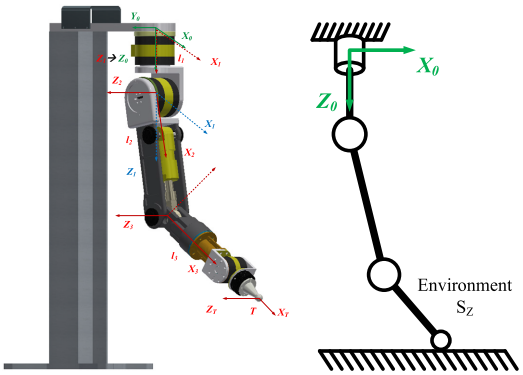

FIGURE 3. Structure and illustration of the 3-DOF serial hydraulic manipulator in the constrained framework.

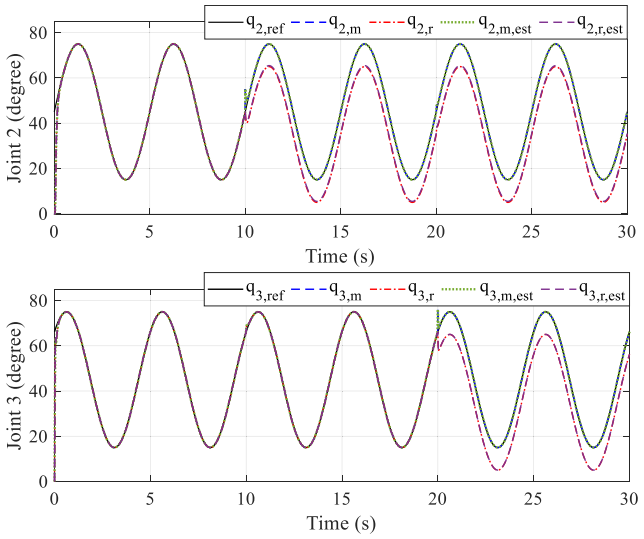

FIGURE 4. Position tracking performance and system state estimation without FTC under the presence of fault signals of joint 2 (up) and joint 3 (down).

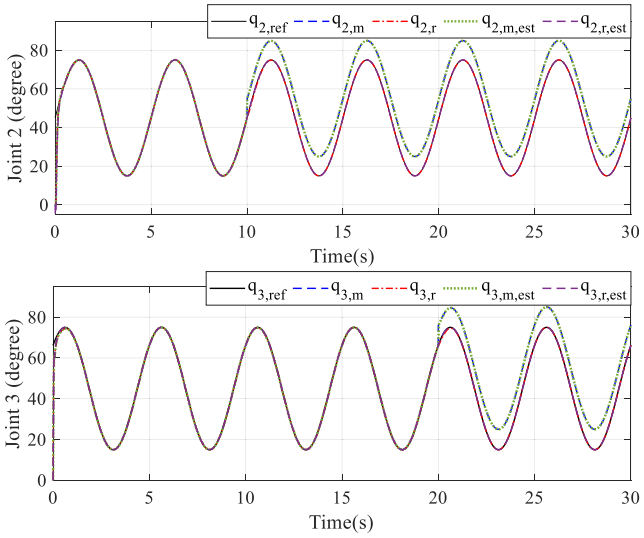

FIGURE 5. Position tracking performance under the FTC-ESO of joint 2 (up) and joint 3 (down).

line denotes the real joint angles $q_{i,r}$, the green dot-dot line denotes the estimated measured joint angles $q_{i,m,est}$, and the purple line denotes the estimated real joint angle $q_{i,r,est}$, with $i = 2,3$. As can be seen in FIGURE 4, when faults occur, since the measured faulty signals are feedback to the controller, the actuator executes the faulty commanded signals; thus, the actual system performance is different from the desired trajectory. Practically, signal faults are unknown; thus, the actual joint angles are not able to be monitored without fault estimation technique since only measured joint angle is available. With the fault estimation method, the actual joint angles and faulty signals are estimated. Then the estimated joint angles are assigned as feedback signals to the main FTC.

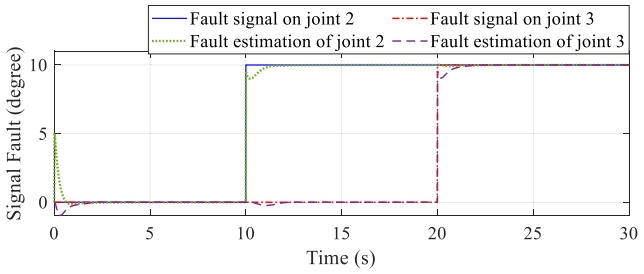

FIGURE 6. Real faults and faults estimation.

The effectiveness of this proposed control scheme is shown in FIGURE 5 in which the actual joint angles are accurately estimated and follow the desired trajectory. The estimation of the faulty signals is shown in FIGURE 6. As the faults of the 2nd joint and 3rd joint occur at the time of 10 and 20 second, respectively, the proposed robust observer can instantly respond to estimate their residual signals. The blue continuous line and red dot-dash line denote the sensor fault signals adding on the 2nd and 3rd joints, respectively; the green dot-dot line and purple dash line denote the estimated sensor fault signals with respect to the homologous real faults, respectively.

2) CASE STUDY 2

In the second case study, the effectiveness of the proposed FTC is verified in the constrained framework. In this scenario, the manipulator is in interaction with the environment in the (S_Z) plane, only normal force in the Z-direction is considered; then, the environment location is given as

$$X_{env,Z} = 0.4\,(m) \tag{41}$$

The desired trajectory and desired interactive force are given by:

$$\mathbf{X}_d = \begin{pmatrix} -\dfrac{2\left(X_{d,Xf} - X_{d,X0}\right)}{t_f^3} t^3 + \dfrac{3\left(X_{d,Xf} - X_{d,X0}\right)}{t_f^2} t^2 + X_{d,X0} \\ -\dfrac{2\left(X_{d,Zf} - X_{d,Z0}\right)}{t_f^3} t^3 + \dfrac{3\left(X_{d,Zf} - X_{d,Z0}\right)}{t_f^2} t^2 + X_{d,Z0} \end{pmatrix}$$

$$= \begin{pmatrix} X_{d,X} \\ X_{d,Z} \end{pmatrix} (m) \tag{42}$$

$$F_{d,Z}(N) = \begin{cases} 0 & \text{if } t < 4.5s \\ 30 & \text{if } 4.5 \le t < 9s \\ 0 & \text{if } 9 \le t < 13s \\ 15 & \text{if } 13 \le t \le 17s \\ 0 & \text{if } t > 17s \end{cases} \tag{43}$$

where $X_{d,X0} = 0.2\,(m)$ and $X_{d,Xf} = 0.85\,(m)$ denote the initial and final points of the desired trajectory along X-direction; $X_{d,Z0} = 0.5\,(m)$ and $X_{d,Zf} = -0.2\,(m)$ denote the initial and final point of the desired trajectory along Z-direction, respectively.

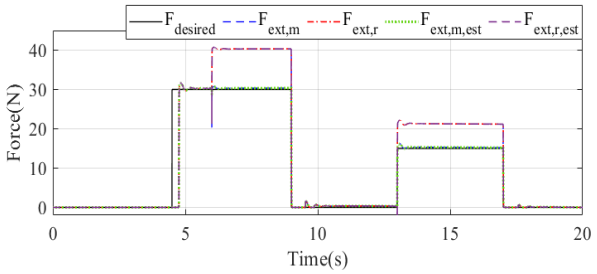

FIGURE 7. Force tracking performance and estimation results without FTC in the presence of sensor fault.

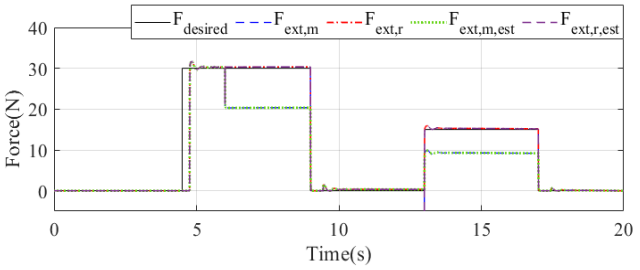

FIGURE 8. Force tracking performance under the FTC with ESO.

In order to illustrate the sensor fault signals, the offset values are added to the feedback force and joint angles. The fault signals of encoder and force sensors are given by:

$$\mathbf{f}_{ss2} = \begin{pmatrix} 0 & 0 & f_{ss2,Z} \end{pmatrix}^T$$
$$f_{ss2,Z} = \begin{cases} 0(N) & \text{if } t < 6s \\ -10(N) & \text{if } 6 \leq t < 12s \\ -6(N) & \text{if } t > 12s \end{cases} \quad (44)$$

It is noteworthy that if the force sensor remains an offset value when the end-effector is not in contact with the environment, it is because of the calibration process. Therefore, the measured interactive force signal is only faulty in the constrained motion when the desired force is not zero. Otherwise, the force sensor returns zero. Moreover, the value of force signal fault cannot abruptly change from zero to any value as discontinuous function, so it is practically reasonable to require a certain time to change this signal fault from zero to the reference value. The parameters of the impedance behaviors are $\mathbf{D}_m = 10\mathbf{I}_2$, $\mathbf{B}_m = 100\mathbf{I}_2$, $\mathbf{K}_m = 500\mathbf{I}_2$, $K_e = 5000$, force control gains are $\mathbf{K}_{Pf} = 4\mathbf{I}_2$, $\mathbf{K}_{If} = 60\mathbf{I}_2$, $\eta_f = 0.5\mathbf{I}_2$; and force observer gains are $\eta_{f2} = 200\mathbf{I}_2$, $\eta_{f3} = 10\mathbf{I}_2$. The initial position of the end-effector is $X_{X0} = -0.2\ (m)$ and $X_{Z0} = 0.5\ (m)$.

The response of the measured force and actual force exerted on the end-effector is shown in FIGURE 7. The negative value of force sensor fault signal in (44) implies that the measured force is less than the actual interactive force. It means the control action attempts to generate more force than necessity without consideration of faulty signal. Practically, the actual interactive force cannot be obtained due to an unknown signal fault. Only measured force, which includes the fault, is measured when using a force sensor.

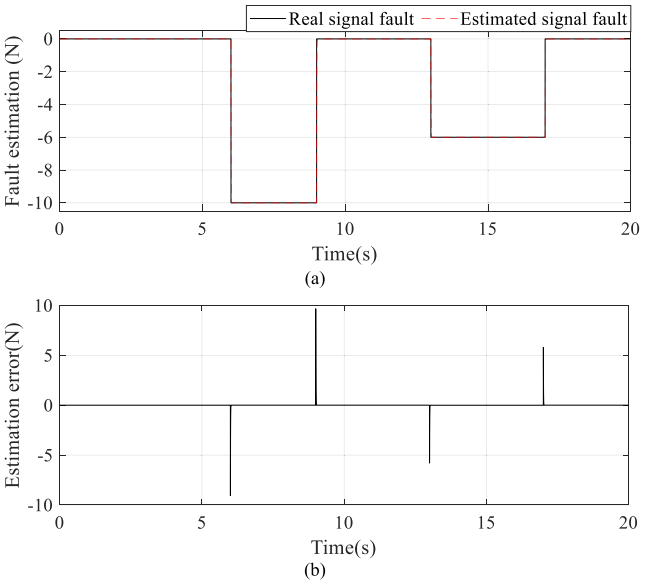

FIGURE 9. Signal fault estimation results: (a) magnitude of the faulty signal, and (b) estimation error.

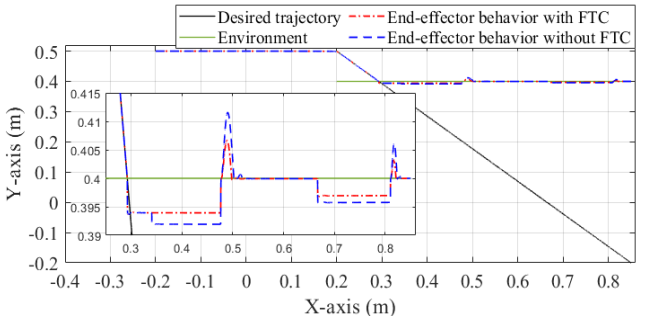

FIGURE 10. End-effector behavior under the presence of force sensor fault in constrained framework environment.

When employing the ESO, the measured force is estimated; thus, the actual force and signal fault are systematically estimated. The black continuous line denotes the desired force $F_{desired}$, the blue dash line denotes the measured interactive force $F_{ext,m}$, the red dot-dash line denotes the real interactive force $F_{ext,r}$, the green dot-dot line denotes the estimation of the measure interactive force $F_{ext,m,est}$, the purple line denotes the estimation of the real interactive force $F_{ext,r,est}$.

With the estimation, the faulty signal is removed and the estimated actual interactive force is feedback to the controller. Consequently, the actual force properly tracks the desired one whereas the measured force is offset by the exact faulty signal, as shown in FIGURE 8. The fault estimation and its estimated error are depicted in FIGURE 9.

FIGURE 10 shows the end-effector performance under the presence of force sensor fault in constrained framework conditions. The black continuous line denotes the originally desired trajectory, the green continuous line denotes the environment, the blue dash line denotes the constrained behavior of the end-effector without FTC, and the red dot-dash line denotes the constrained behavior of the end-effector with the FTC. As can be compared, the difference of real

exerted interactive force results in the difference in the real end-effector behavior. With the force sensor fault estimation and FTC, the end-effector performance is the same as the case of fault-free condition.

VI. CONCLUSION

This paper proposed a novel fault estimation algorithm to detect and estimate both encoder and force sensor faults on the n-DOF serial hydraulic manipulator subjected to constrained framework conditions. These faults may originate from practical setup calibration or accommodation of measured signal offset due to long-term usage, or malfunction. To address the influence of the sensor faults, the fault estimation algorithm based on ESO was designed to detect and estimate the measured and actual joint angle and force faulty signals. In order to exhibit more fast convergence and estimation accuracy, some remarks with modified updating laws were introduced. Then, the estimated force was feedback to the impedance control block and the estimated actual joint angles were feedback to the main controller. Based on the feedback estimated variables, the robust FTC-based FBSMC scheme was designed to execute the suitable action on the actuators. The stability of the proposed ESO and closed-loop system is mathematically proven by performing the Lyapunov theorems. The comparative simulations on the 3-DOF serial hydraulic manipulator verified the effectiveness of the proposed algorithm in instantly detecting and estimating the faulty residuals. With the advantage of the ESO, the real actual interactive force can be online estimated; thereby, force-sensorless-based ESO can be certainly implemented to replace the use of force sensors. This paper can be considered as a premise, with some remaining limitations pertaining to assumptions to facilitate the control methodology design, for further development as

1) Consideration of environment characteristics. In this manuscript, the environment damping, friction, and environment characteristics in general, were ignored to simplify the calculation and facilitate the proposed control methodology. Practically, the influence of the environment characteristics shall be taken into consideration as a factor to enhance the system performance.
2) The forward kinematic in the ESO in (16) will be carefully considered as a nonlinear term instead of being approximated as linear calculus by Lipchitz in Assumption 6. In this sense, the matrices Ai in (23) and (24) becomes time-varying nonlinear matrices. This may complicate the calculation; however, the system behaviors will be described to its true nature.
3) Analysis of simultaneous faults of joint angle and interactive force. In this event, a problem happens when the end-effector is in contact with the environment, but the fault arising on either joint angle sensor or force sensor lifts the end-effector off the working surface. This conflict between the contact and contact-lost shall be clarified.
4) Consideration of pressure sensor fault because this fault can cause a threat as same as the actuator fault and the phenomenon may not be clearly displayed and easily detected. This issue was indicated by Nahian *et al.* [30]; however, the author limited the scope where only one pressure sensor fault in the head-side of the cylinder and a linear sensor fault were taken into consideration. Indeed, when one pressure sensor is faulty, abnormal signals of both sensors are all obtained. So, it is difficult to identify which sensor is really faulty in this case.
5) Integration of hybrid observers, or adaptive observer gains to effectively estimate different types of disturbances based on their characteristics. In this case, the robustness of the estimator subjects to noise or unexpected signals impact shall be carefully studied [59], [60].

Consequently, the above potential threats may evoke interesting topics for further developments.

APPENDIX

PROOF OF THEOREM 1

Consider the Lyapunov candidate $V_{ESO,1}$ as

$$V_{ESO,1} = \frac{1}{2}\varepsilon_1^T \mathbf{P}_1 \varepsilon_1 \tag{45}$$

Taking the derivative of the $V_{ESO,1}$ yields:

$$\dot{V}_{ESO,1} = \frac{1}{2}\dot{\varepsilon}_1^T \mathbf{P}_1 \varepsilon_1 + \frac{1}{2}\varepsilon_1^T \mathbf{P}_1 \dot{\varepsilon}_1 \tag{46}$$

Apply the dynamics (23) into (46), the derivative of the $V_{ESO,1}$ becomes:

$$\begin{aligned}\dot{V}_{ESO,1} &= \frac{1}{2}\left(\frac{1}{\sigma_1}\varepsilon_1^T \mathbf{A}_1^T + \sigma_1^2 \mathbf{H}_1^T \mathbf{B}_1^T\right)\mathbf{P}_1 \varepsilon_1 \\ &\quad + \frac{1}{2}\varepsilon_1^T \mathbf{P}_1 \left(\frac{1}{\sigma_1}\mathbf{A}_1 \varepsilon_1 + \sigma_1^2 \mathbf{B}_1 \mathbf{H}_1\right) \\ &= \frac{1}{2\sigma_1}\varepsilon_1^T \left(\mathbf{A}_1^T \mathbf{P}_1 + \mathbf{P}_1 \mathbf{A}_1\right)\varepsilon_1 + \sigma_1^2 \varepsilon_1^T \mathbf{P}_1 \mathbf{B}_1 \mathbf{H}_1\end{aligned} \tag{47}$$

Applying Young's inequality into (47) results in:

$$\begin{aligned}\dot{V}_{ESO,1} &\le -\frac{1}{2\sigma_1}\varepsilon_1^T \mathbf{I}_{3n+3}\varepsilon_1 + \frac{1}{2}\sigma_1^2 \varepsilon_1^T \mathbf{P}_1^T \mathbf{B}_1 \mathbf{B}_1^T \mathbf{P}_1 \boldsymbol{\varepsilon}_1 \\ &\quad + \frac{1}{2}\sigma_1^2 \mathbf{H}_1^T \mathbf{H}_1 \\ &\le -\frac{1}{2}\left(\frac{1}{\sigma_1} - \sigma_1^2 \lambda_{\max}\left(\mathbf{P}_1^T \mathbf{B}_1 \mathbf{B}_1^T \mathbf{P}_1\right)\right)\|\varepsilon_1\|^2 \\ &\quad + \frac{1}{2}\sigma_1^2 \mathbf{H}_1^T \mathbf{H}_1\end{aligned} \tag{48}$$

$$\dot{V}_{ESO,1} \le -\gamma_{ESO,1} V_{ESO,1} + \Delta_{ESO,1} \tag{49}$$

By choosing a small value of σ_1, the derivative of the Lyapunov candidate $V_{ESO,1}$ becomes semi-negative. Therefore, theorem 1 is proven. The Lyapunov candidate $V_{ESO,1}$ is UUB and converges to the bound:

$$V_{ESO,1} \le V_{ESO,1}(0)\, e^{-\gamma_{ESO,1} t} + \frac{\Delta_{ESO,1}}{\gamma_{ESO,1}}\left(1 - e^{-\gamma_{ESO,1} t}\right) \tag{50}$$

where $\gamma_{ESO,1} = \min\left(\frac{1}{2}\left(\frac{1}{\sigma_1} - \sigma_1^2\lambda_{\max}\left(\mathbf{P}_1^T\mathbf{B}_1\mathbf{B}_1^T\mathbf{P}_1\right)\right)\right)$, $\Delta_{ESO,1} = \frac{1}{2}\sigma_1^2\mathbf{H}_1^T\mathbf{H}_1$.

Following the above calculation, theorem 2 is proven.

REFERENCES

[1] V. T. Yen, W. Y. Nan, and P. Van Cuong, "Robust adaptive sliding mode neural networks control for industrial robot manipulators," *Int. J. Control, Autom. Syst.*, vol. 17, no. 3, pp. 783–792, Mar. 2019.

[2] H. Wen, M. Cong, G. Wang, W. Qin, W. Xu, and Z. Zhang, "Dynamics and optimized torque distribution based force/position hybrid control of a 4-DOF redundantly actuated parallel robot with two point-contact constraints," *Int. J. Control, Autom. Syst.*, vol. 17, no. 5, pp. 1293–1303, May 2019.

[3] D. T. Tran, D. X. Ba, and K. K. Ahn, "Adaptive backstepping sliding mode control for equilibrium position tracking of an electrohydraulic elastic manipulator," *IEEE Trans. Ind. Electron.*, vol. 67, no. 5, pp. 3860–3869, May 2020.

[4] M. N. Nguyen, D. T. Tran, and K. K. Ahn, "Robust position and vibration control of an electrohydraulic series elastic manipulator against disturbance generated by a variable stiffness actuator," *Mechatronics*, vol. 52, pp. 22–35, Jun. 2018.

[5] H. T. Do, T. D. Dang, H. V. A. Truong, and K. K. Ahn, "Maximum power point tracking and output power control on pressure coupling wind energy conversion system," *IEEE Trans. Ind. Electron.*, vol. 65, no. 2, pp. 1316–1324, Feb. 2018.

[6] D. T. Tran, H. V. Dao, T. Q. Dinh, and K. K. Ahn, "Output feedback control via linear extended state observer for an uncertain manipulator with output constraints and input dead-zone," *Electronics*, vol. 9, no. 9, p. 1355, Aug. 2020.

[7] D.-T. Tran, T.-C. Do, and K.-K. Ahn, "Extended high gain observer-based sliding mode control for an electro-hydraulic system with a variant payload," *Int. J. Precis. Eng. Manuf.*, vol. 20, no. 12, pp. 2089–2100, Dec. 2019.

[8] T. C. Do, D. T. Tran, T. Q. Dinh, and K. K. Ahn, "Tracking control for an electro-hydraulic rotary actuator using fractional order fuzzy PID controller," *Electronics*, vol. 9, no. 6, p. 926, Jun. 2020.

[9] D. Li, L. Wei, T. Song, and Q. Jin, "Study on asymptotic stability of fractional singular systems with time delay," *Int. J. Control, Autom. Syst.*, vol. 18, no. 4, pp. 1002–1011, Apr. 2020.

[10] D.-K. Gu, L.-W. Liu, and G.-R. Duan, "A parametric method of linear functional observers for linear time-varying systems," *Int. J. Control, Autom. Syst.*, vol. 17, no. 3, pp. 647–656, Mar. 2019.

[11] H.-V.-A. Truong, D.-T. Tran, and K. K. Ahn, "A neural network based sliding mode control for tracking performance with parameters variation of a 3-DOF manipulator," *Appl. Sci.*, vol. 9, no. 10, p. 2023, May 2019.

[12] H. V. A. Truong, D. T. Tran, X. D. To, K. K. Ahn, and M. Jin, "Adaptive fuzzy backstepping sliding mode control for a 3-DOF hydraulic manipulator with nonlinear disturbance observer for large payload variation," *Appl. Sci.*, vol. 9, no. 16, p. 3290, Aug. 2019.

[13] D.-T. Tran, M.-N. Nguyen, and K. K. Ahn, "RBF neural network based backstepping control for an electrohydraulic elastic manipulator," *Appl. Sci.*, vol. 9, no. 11, p. 2237, May 2019.

[14] D.-T. Tran, H.-V.-A. Truong, and K. K. Ahn, "Adaptive backstepping sliding mode control based RBFNN for a hydraulic manipulator including actuator dynamics," *Appl. Sci.*, vol. 9, no. 6, p. 1265, Mar. 2019.

[15] D. T. Tran, M. Jin, and K. K. Ahn, "Nonlinear extended state observer based on output feedback control for a manipulator with time-varying output constraints and external disturbance," *IEEE Access*, vol. 7, pp. 156860–156870, 2019.

[16] H. J. Yoon, S. Y. Chung, and M. J. Hwang, "Shadow space modeling and task planning for collision-free cooperation of dual manipulators for planar task," *Int. J. Control, Autom. Syst.*, vol. 17, no. 4, pp. 995–1006, Apr. 2019.

[17] Y. Yang and B. Ding, "An iterative optimization approach for fuzzy predictive control," *Int. J. Control, Autom. Syst.*, vol. 18, no. 8, pp. 2157–2164, Aug. 2020.

[18] H. A. Trinh, H. V. A. Truong, and K. K. Ahn, "Fault estimation and fault-tolerant control for the pump-controlled electrohydraulic system," *Actuators*, vol. 9, no. 4, p. 132, Dec. 2020.

[19] H. V. Dao, D. T. Tran, and K. K. Ahn, "Active fault tolerant control system design for hydraulic manipulator with internal leakage faults based on disturbance observer and online adaptive identification," *IEEE Access*, vol. 9, pp. 23850–23862, 2021, doi: 10.1109/ACCESS.2021.3053596.

[20] T. X. Dinh, T. D. Thien, T. H. V. Anh, and K. K. Ahn, "Disturbance observer based finite time trajectory tracking control for a 3 DOF hydraulic manipulator including actuator dynamics," *IEEE Access*, vol. 6, pp. 36798–36809, 2018.

[21] D. X. Ba, T. Q. Dinh, J. Bae, and K. K. Ahn, "An effective disturbance-observer-based nonlinear controller for a pump-controlled hydraulic system," *IEEE/ASME Trans. Mechatronics*, vol. 25, no. 1, pp. 32–43, Feb. 2020.

[22] M. Homayounzade and A. Khademhosseini, "Disturbance observer-based trajectory following control of robot manipulators," *Int. J. Control, Autom. Syst.*, vol. 17, no. 1, pp. 203–211, Jan. 2019.

[23] Y. Xin, X. Rong, Y. Li, B. Li, and H. Chai, "Movements and balance control of a wheel-leg robot based on uncertainty and disturbance estimation method," *IEEE Access*, vol. 7, pp. 133265–133273, 2019.

[24] B. Ren, Q.-C. Zhong, and J. Chen, "Robust control for a class of nonaffine nonlinear systems based on the uncertainty and disturbance estimator," *IEEE Trans. Ind. Electron.*, vol. 62, no. 9, pp. 5881–5888, Sep. 2015.

[25] J. Choi, J. Baek, W. Lee, Y. S. Lee, and S. Han, "Adaptive model-free control with nonsingular terminal sliding-mode for application to robot manipulators," *IEEE Access*, vol. 8, pp. 169897–169907, 2020.

[26] J. Lee, P. H. Chang, and M. Jin, "An adaptive gain dynamics for time delay control improves accuracy and robustness to significant payload changes for robots," *IEEE Trans. Ind. Electron.*, vol. 67, no. 4, pp. 3076–3085, Apr. 2020.

[27] Y. Wang, S. Meng, F. Ju, B. Chen, and H. Wu, "A novel model-free robust control of cable-driven manipulators," *IEEE Access*, vol. 7, pp. 125532–125541, 2019.

[28] M. Bahrami, M. Naraghi, and M. Zareinejad, "Adaptive super-twisting observer for fault reconstruction in electro-hydraulic systems," *ISA Trans.*, vol. 76, pp. 235–245, May 2018.

[29] M. H. Amoozgar, A. Chamseddine, and Y. Zhang, "Experimental test of a two-stage Kalman filter for actuator fault detection and diagnosis of an unmanned quadrotor helicopter," *J. Intell. Robotic Syst.*, vol. 70, nos. 1–4, pp. 107–117, Apr. 2013.

[30] S. A. Nahian, T. Q. Dinh, H. V. Dao, and K. K. Ahn, "An unknown input observer–EFIR combined estimator for electrohydraulic actuator in sensor fault-tolerant control application," *IEEE/ASME Trans. Mechatronics*, vol. 25, no. 5, pp. 2208–2219, Oct. 2020.

[31] V. D. Phan, C. P. Vo, H. V. Dao, and K. K. Ahn, "Robust fault-tolerant control of an electro-hydraulic actuator with a novel nonlinear unknown input observer," *IEEE Access*, vol. 9, pp. 30750–30760, 2021, doi: 10.1109/ACCESS.2021.3059947.

[32] M. H. Nguyen, H. V. Dao, and K. K. Ahn, "Active disturbance rejection control for position tracking of electro-hydraulic servo systems under modeling uncertainty and external load," *Actuators*, vol. 10, no. 2, p. 20, Jan. 2021.

[33] Y. Huang and W. Xue, "Active disturbance rejection control: Methodology and theoretical analysis," *ISA Trans.*, vol. 53, no. 4, pp. 963–976, Jul. 2014.

[34] M. Van, S. Sam Ge, and H. Ren, "Robust fault-tolerant control for a class of second-order nonlinear systems using an adaptive third-order sliding mode control," *IEEE Trans. Syst., Man, Cybern. Syst.*, vol. 47, no. 2, pp. 221–228, Feb. 2017.

[35] M. Van, X. P. Do, and M. Mavrovouniotis, "Self-tuning fuzzy PID-nonsingular fast terminal sliding mode control for robust fault tolerant control of robot manipulators," *ISA Trans.*, vol. 96, pp. 60–68, Jan. 2020.

[36] A. T. Vo and H.-J. Kang, "A novel fault-tolerant control method for robot manipulators based on non-singular fast terminal sliding mode control and disturbance observer," *IEEE Access*, vol. 8, pp. 109388–109400, 2020.

[37] V. Reppa, M. M. Polycarpou, and C. G. Panayiotou, "Adaptive approximation for multiple sensor fault detection and isolation of nonlinear uncertain systems," *IEEE Trans. Neural Netw. Learn. Syst.*, vol. 25, no. 1, pp. 137–153, Jan. 2014.

[38] T. Van Nguyen and C. Ha, "Experimental study of sensor fault-tolerant control for an electro-hydraulic actuator based on a robust nonlinear observer," *Energies*, vol. 12, no. 22, p. 4337, Nov. 2019.

[39] T. Van Nguyen and C. Ha, "Sensor fault-tolerant control design for mini motion package electro-hydraulic actuator," *Processes*, vol. 7, no. 2, p. 89, Feb. 2019.

[40] S. A. Nahian, D. Q. Truong, P. Chowdhury, D. Das, and K. K. Ahn, "Modeling and fault tolerant control of an electro-hydraulic actuator," *Int. J. Precis. Eng. Manuf.*, vol. 17, no. 10, pp. 1285–1297, Oct. 2016.

[41] D. Brambilla, L. M. Capisani, A. Ferrara, and P. Pisu, "Fault detection for robot manipulators via second-order sliding modes," *IEEE Trans. Ind. Electron.*, vol. 55, no. 11, pp. 3954–3963, Nov. 2008.

[42] L. M. Capisani, A. Ferrara, A. Ferreira de Loza, and L. M. Fridman, "Manipulator fault diagnosis via higher order sliding-mode observers," *IEEE Trans. Ind. Electron.*, vol. 59, no. 10, pp. 3979–3986, Oct. 2012.
[43] G. Paviglianiti, F. Pierri, F. Caccavale, and M. Mattei, "Robust fault detection and isolation for proprioceptive sensors of robot manipulators," *Mechatronics*, vol. 20, no. 1, pp. 162–170, Feb. 2010.
[44] H. Pang, Y. Shang, and P. Wang, "Design of a sliding mode observer-based fault tolerant controller for automobile active suspensions with parameter uncertainties and sensor faults," *IEEE Access*, vol. 8, pp. 186963–186975, 2020.
[45] J. Wang, F. Fang, X. Yi, and Y. Liu, "Dynamic event-triggered fault estimation and sliding mode fault-tolerant control for networked control systems with sensor faults," *Appl. Math. Comput.*, vol. 389, Jan. 2021, Art. no. 125558.
[46] D. Li, Y. Wang, J. Wang, C. Wang, and Y. Duan, "Recent advances in sensor fault diagnosis: A review," *Sens. Actuators A, Phys.*, vol. 309, Jul. 2020, Art. no. 111990.
[47] Y. Sun, Y. Xia, J. Zhang, and D.-W. Ding, "Adaptive fault-tolerant output regulation of linear multi-agent systems with sensor faults," *IEEE Access*, vol. 8, pp. 159440–159448, 2020.
[48] K. Zhang, B. Jiang, and V. Cocquempot, "Adaptive observer-based fast fault estimation," *Int. J. Control Autom. Syst.*, vol. 6, no. 3, pp. 320–326, 2008.
[49] H. Khebbache, S. Labiod, and M. Tadjine, "Adaptive sensor fault-tolerant control for a class of multi-input multi-output nonlinear systems: Adaptive first-order filter-based dynamic surface control approach," *ISA Trans.*, vol. 80, pp. 89–98, Sep. 2018.
[50] B. Siciliano and L. Villani, "Introduction," in *Robot Force Control*, 1st ed. New York, NY, USA: Springer, 1999, ch. 1, pp. 1–6.
[51] J. Duan, Y. Gan, M. Chen, and X. Dai, "Adaptive variable impedance control for dynamic contact force tracking in uncertain environment," *Robot. Auto. Syst.*, vol. 102, pp. 54–65, Apr. 2018.
[52] H. V. A. Truong, H. A. Trinh, and K. K. Ahn, "Safety operation of n-DOF serial hydraulic manipulator in constrained motion with consideration of contact-loss fault," *Appl. Sci.*, vol. 10, no. 22, p. 8107, Nov. 2020.
[53] A. Levant, "Higher-order sliding modes, differentiation and output-feedback control," *Int. J. Control*, vol. 76, nos. 9–10, pp. 924–941, Jan. 2003.
[54] J. Na, Y. Li, Y. Huang, G. Gao, and Q. Chen, "Output feedback control of uncertain hydraulic servo systems," *IEEE Trans. Ind. Electron.*, vol. 67, no. 1, pp. 490–500, Jan. 2020.
[55] W. Deng and J. Yao, "Extended-state-observer-based adaptive control of electrohydraulic servomechanisms without velocity measurement," *IEEE/ASME Trans. Mechatronics*, vol. 25, no. 3, pp. 1151–1161, Jun. 2020.
[56] J. Yao, Z. Jiao, and D. Ma, "Extended-state-observer-based output feedback nonlinear robust control of hydraulic systems with backstepping," *IEEE Trans. Ind. Electron.*, vol. 61, no. 11, pp. 6285–6293, Nov. 2014.
[57] J. Yao and W. Deng, "Active disturbance rejection adaptive control of hydraulic servo systems," *IEEE Trans. Ind. Electron.*, vol. 64, no. 10, pp. 8023–8032, Oct. 2017.
[58] W. Deng, J. Yao, Y. Wang, X. Yang, and J. Chen, "Output feedback backstepping control of hydraulic actuators with valve dynamics compensation," *Mech. Syst. Signal Process.*, vol. 158, Sep. 2021, Art. no. 107769.
[59] Y. Chen, J. Ma, P. Zhang, F. Liu, and S. Mei, "Robust state estimator based on maximum exponential absolute value," *IEEE Trans. Smart Grid*, vol. 8, no. 4, pp. 1537–1544, Jul. 2017, doi: 10.1109/TSG.2015.2485280.
[60] Y. Chen, Y. Yao, and Y. Zhang, "A robust state estimation method based on SOCP for integrated electricity-heat system," *IEEE Trans. Smart Grid*, vol. 12, no. 1, pp. 810–820, Jan. 2021, doi: 10.1109/TSG.2020.3022563.

HOAI VU ANH TRUONG received the B.S. degree in mechanical engineering from the Ho Chi Minh City University of Technology, Ho Chi Minh City, Vietnam, in 2015. He is currently pursuing the Ph.D. degree in mechanical and automotive engineering, University of Ulsan, Ulsan, South Korea. His research interests include renewable energy, energy conversion systems, energy management for hybrid power sources, advanced control and intelligent control for nonlinear systems, nonlinear observers, fault-tolerant control, and robotic manipulator.

HOAI AN TRINH received the B.S. and M.S. degrees in electrical and electronic engineering from the Ho Chi Minh City University of Technology and Education, Ho Chi Minh City, Vietnam, in 2012 and 2015, respectively. He is currently pursuing the Ph.D. degree in the School of Mechanical and Automotive Engineering, University of Ulsan, South Korea. His research interests include robotic systems, nonlinear control, fault-tolerant control, and energy management for hybrid power sources.

DUC THIEN TRAN (Member, IEEE) received the B.S. and M.S. degrees from the Department of Electrical Engineering, Ho Chi Minh City University of Technology, Vietnam, in 2010 and 2013, respectively, and the Ph.D. degree from the University of Ulsan, in 2020.

He works as a Lecturer with the Department of Automatic Control, Ho Chi Minh City University of Technology and Education (HCMUTE), Vietnam. His research interests include robotics, variable stiffness systems, fluid power control, disturbance observer, nonlinear control, adaptive control, and intelligent technique.

KYOUNG KWAN AHN (Senior Member, IEEE) received the B.S. degree from the Department of Mechanical Engineering, Seoul National University, in 1990, the M.Sc. degree in mechanical engineering from the Korea Advanced Institute of Science and Technology (KAIST), in 1992, and the Ph.D. degree from the Tokyo Institute of Technology, in 1999.

Since 2000, he has been with the School of Mechanical Engineering, University of Ulsan, where he is currently a Professor and the Director of the Fluid Power Control and Machine Intelligence Laboratory. He is the author or coauthor of over 190 SCI(E) articles and four books in these areas. His main research interests include fluid-based triboelectric nano generator, modeling and control of fluid power systems, energy saving construction machine, hydraulic robot, and power transmission in the ocean energy.

Dr. Ahn serves as an Editor for *International Journal of Control, Automation and Systems*, and Editorial Board Member for *Renewable Energy*, *Korean Fluid Power and Construction Machine*, and *Actuators*.